Insights into the active catalyst formation in palladium catalyzed coupling reaction from di-nuclear palladium acetate: A DFT study

Saikat Roy[1] and Anakuthil Anoop[1*]

[1]*Department of Chemistry, Indian Institute of Technology Kharagpur, 721302*

E-mail: anoop@chem.iitkgp.ac.in

Abstract

We explored the formation of active palladium catalyst species by degradation of Pd-acetate dimer with the addition of phosphine ligands (PH_3 and PPh_3) with an automated reaction search employing Density Functional Theory calculations followed by kinetic studies with stochastic simulation analysis. Our reaction search starting from dimeric form, considered a resting state of the catalyst, produced similar monomeric species by sequential ligand addition as found in the experimental investigation of the active catalytic species in Heck reactions. We analyzed the bonding in the Pd-acetate dimer and the role of Pd in the stability of the dimeric species. We implemented the Gillespie Stochastic Simulation Algorithm and applied it to the degradation reaction path. This algorithm can give more insights into multi-channel reaction paths. The energetics of the degradation path is reasonably achievable in the experimental reaction conditions that make dimeric species a potential catalytic precursor in the Pd-acetate catalyzed coupling reactions.

Introduction

Palladium-based catalysts continue to be the most competent transition-metal catalysts and are the most sophisticated tools for the carbon-carbon bond formation reactions.[1] Several unique features of Pd makes it catalytically effective, e.g., it can form complexes in various oxidation states (0, I, II, III, and IV)[2] can behave as a redox-neutral center in various coupling reactions, can facilitate high substrate binding and release via ligand exchange, and most importantly, these reactions usually proceed with a high product yield percentage using a tiny amount (ppm to ppb) amount of Pd catalyst.

The active palladium catalyst may exist in any of the many possible catalyst forms in the catalytic process. For example, the Pd center may be mono/di/tri ligated or ligand-free, and the metal center may be formally neutral, cationic, or anionic, depending on the ligand or reaction condition. Common precursors in use are $Pd(OAc)_2$, $Pd(PR_3)_4$, $PdCl_2(PR_3)_2$ etc. In the ligand-free Heck reactions, one of the active catalysts is Pd nanoparticles.[3] $PdCl_2$ or $[Pd(OAc)_2]_3$ are the most common precursors. Strong donor polar solvents (e.g., DMF, THF) cause the breakdown of solid-state trimeric $[Pd(OAc)_2]_3$ structure. Two sequential processes are observed, using UV-Vis spectroscopy, during the breakdown process. When water is added to a THF solution, the trimer disaggregates first, and then the hydrolysis of $Pd(OAc)_2$ gives AcOPdOH. The AcOPdOH species is unstable and leads to the formation of Pd nanoparticles. The addition of phenylboronic acid can accelerate this nanoparticle formation. Sulfonic acids can replace acetate from $Pd(OAc)_2$ and form more electrophilic $Pd(OTs)_2$ and $Pd(OTf)_2$.

While palladium acetate is a versatile catalyst precursor,[4] there is much to be learned about the mechanism of its transformation to active catalyst species. The actual resting state of palladium acetate is still a matter of debate. Palladium acetate might exist as mononuclear $Pd(OAc)_2$, bi-nuclear $[Pd(OAc)_2]_2$ or trinuclear $[Pd(OAc)_2]_3$ depending upon various external parameters such as solvent property, experimental temperature, concentration. The X-ray study of the palladium acetate crystal reveals that palladium acetate mainly exists as trinuclear species in solid form.[5] However, it could exist in the monomeric or dimeric form in the solution phase, depending upon the dilution and external coordinating solvent. For example, Ritter[6,7] and Sanford[8] proposed that dinuclear Pd(III) are the intermediates instead of mononuclear Pd(IV) in C-H functionalization reaction. Schoenebeck and co-workers[9] have shown that $[(P^tBu_3)PdBr]_2$ dimer reacts with aryl iodide as a dinuclear species while mononuclear Pd(0) species react with aryl chlorides and bromides, and the nature of the active catalytic component depends on the conditions of the reaction, including solvent and additives. Cook and Sanford[10] have demonstrated that in nondirected arene C-H acetoxylation reaction, a 1:1 mixture of $Pd(OAc)_2$ and pyridine (catalyst to ligand) forms a dimeric Pd(II) species that immediately converted to the coordinatively unsaturated monomeric Pd(II) active catalyst. Identifying the nature of pre-catalyst and active species in these coupling reactions is essential to understanding the reactivity and selectivity of the reactions.

Amatore and Jutand, in their seminal work, studied the oxidative addition step in cross-coupling reactions by electrochemical tracking of Pd(0) species. This work has been carried out by ^{31}P NMR studies. They showed that with excess PPh_3 (and H_2O), the reduction of $Pd(OAc)_2$ leads to the formation of anionic species $Pd(PPh_3)_nOAc^-$, where n depends on the concentration of phosphine. The intermediate species rapidly react to PhI and form trans-$PhPd(PPh_3)OAc$ and iodide ions. This product and its equilibrium with I^- has been verified by NMR. They also suggested the following reaction mechanism for the reduction of $Pd(OAc)_2$ by PPh_3:

$$\begin{aligned} &Pd(OAc)_2 + 2PPh_3 \rightarrow Pd(OAc)_2(PPh_3)_2, \quad \text{fast} \\ &Pd(OAc)_2(PPh_3)_2 \rightarrow Pd^0(PPh_3)(OAc)^- + AcO\text{-}PPh_3{}^+ \\ &Pd^0(PPh_3)(OAc)^- + PPh_3 \rightarrow Pd^0(PPh_3)_2(OAc)^-, \quad \text{fast} \\ &Pd^0(PPh_3)_2(OAc)^- + PPh_3 \rightarrow Pd^0(PPh_3)_3(OAc)^-, \quad \text{fast} \end{aligned} \tag{1}$$

The existence and stability of these anionic Pd(0) intermediates ($[Pd(PPh_3)_n(OAc)_2]^-$; n = 2,3) have been investigated experimentally[11] and by theoretical calculations.[12,13]

Until now, most of the computational studies on resolving the mechanism of $Pd(OAc)_2$ catalyzed Heck reaction have considered mononuclear $Pd(OAc)_2$ as the initial catalyst, which might be a reasonable assumption in some reaction conditions. However, palladium acetate dimer as a potential resting state of the active catalyst cannot be ruled out. Very few computational studies consider the dimeric form of $Pd(OAc)_2$ as the resting state of the active catalyst.[14,15]

To understand the breakdown of Pd-acetate-dimer into monomeric Pd acetate and other potential active catalyst species, we have studied the possible pathways using density functional theory calculations. We started with $[Pd(OAc)_2]_2$ dimeric complex as a pre-catalyst and explored its reaction with the sequentially added PH_3 and PPh_3 ligands till the formation of monomeric Pd complexes. To facilitate the discovery of several possible pathways and intermediates, we employed an automated reaction finding method developed in our group.[16] This automated method which is based on the AFIR method[17,18] generates several possible intermediates in each step when the Pd di-nuclear species decomposed to monomeric species. We calculated the energy barrier for the formation of each intermediate to compare the pathways and understand the feasibility of these steps. After the formation of several mononuclear Pd species, we simulated the kinetic process with the help of Gillespie's Stochastic Simulation Algorithm (SSA).[19] We have employed the SSA to identify the major products in a multi-channel reaction mechanism path.

Computational Methods

We have generated many possible intermediates with the addition of PH_3 to Pd-acetate dimer in each subsequent step using the Tabu-search-based algorithm[16] described in the SI (Page S-1). Among all the intermediates generated by this automated search method, we choose only those geometries where the newly incoming PH_3 coordinated to any Pd centers. To these selected intermediates, we have added the next PH_3. This process is continued till the bridged structure is broken into monomeric structures. For the addition of PPh_3s, we modeled the intermediates with PPh_3 ligand in place of PH_3 manually and performed the following methods to locate the transition states.

The energy and the gradient computations in the automated search method were performed with XTB[20] software with semiempirical GFN-xTB[21] method. Optimization with the artificial force was carried out by using the statpt module implemented in Turbomole[22] with RI-BP86[23] level of theory with D3[24] dispersion correction. After getting the intermediates from the automated search for each step, we performed a relaxed surface scan with Pd-P distance as the reaction coordinate. In each step of the scan, only the Pd-P distance was kept constant while all other coordinates were fully relaxed. We increased the Pd-P distance by 0.5 Å in each step, and the last geometry of the scan was fully relaxed without any constraint. After we got the initially optimized geometries of both sides, the transition state guess geometries were located by the climbing-image nudged elastic band[25] (CI-NEB) method implemented in ORCA.[26] Vibrational frequency calculations were performed on all the optimized geometries, and we characterized the reactants and intermediates with no imaginary frequency and one imaginary frequency corresponding to reaction mode for transition state geometries. In addition, intrinsic reaction coordinate (IRC) calculations were carried out to confirm the minimum reaction path.

Optimization and frequency analysis of the geometries were performed with the ORCA package with RI[27]-TPSS[28]/def2-SVP[29] level of theory with Grimme's D3[24] dispersion correction with BJ[30] damping. The default effective core potential (def2-ecp[31]) was used for the relativistic effects for the Pd atom. The natural atomic orbital (NAO[32]) method was used to find out the molecular orbital composition with the Multiwfn[33] package. NAO calculations were performed using the NBO 3.1 from the Gaussian[34] software.

We have carried out the kinetic studies using the Stochastic Simulation Algorithm (SSA) to understand the behavior of our system containing multi-channel reaction pathways. The background of the theory and the details of our implementation are given in the Supporting Information (S-2). A description of the input and output of the program is given below.

Parameters of the stochastic algorithm are parsed from the input file in *YAML* format. A sample input file is provided in the Supporting Information (S-5). The input parameters are **Temp**(temperature in kelvin), **Steps**(Number of Monte Carlo Steps), **Initial_pop**(Initial population of the reactive species), and **Stoichiometry**(Stoichiometry matrix). Each row of the stoichiometry matrix consists of a list of two python-lists. The first one is the Gibbs Free energy of activation ($\Delta G^{\dagger}$), and the second list is the corresponding elementary reaction. Each elementary reaction is denoted by three values **0, +1,** and **-1**. If a species is consumed in a particular elementary reaction, then the corresponding value is **-1**, and it is **+1** where it is produced. If any species that are not involved in that particular elementary reaction or it is concentration is not affected by that elementary reaction, then those values are **0** in the row of the stoichiometry matrix. The total number of elements in each matrix row is equal to the total number of species that are mentioned in the **Initial_pop** section of the *YAML* input file and the total number of columns is equal to the total number of elementary reactions involved in the system. The number of monte Carlo steps can control the simulation length.

The SSA code gives the output in *CSV* file format. The first element is the time, and the following elements are the populations of each species (**Initial_pop**) at that particular point in time. The order of populations in the *CSV* output is the same as the order of **Initial_pop** of the *YAML* input file. The data in the *CSV* file can be plotted later in any software/packages (e.g., python-matplotlib). The time step of the simulation (dt) is hard-coded in the SSA code.

Results and discussions

Structure and Bonding Analysis of dimeric $[Pd(OAc)_2]_2$

The crystal structure of palladium acetate showed that Pd-acetate exists in the trimeric form $[Pd(OAc)_2]_3$ in the absence of other coordinating ligands. Each of the three Pd atoms in $[Pd(OAc)_2]_3$ is in the square planner arrangement. We have optimized the trimeric structure (Figure 1), which is in good agreement with the reported crystal structure.[5] Minor structural differences are expected due to crystal packing and other factors.

Musaev and co-workers[35] calculated that the transformation from trimeric form to dimeric form is unfavorable by 17.4 kcal mol^{-1} at M06[36]/[6-31G(d,p)[37]+Lanl2dz[38–40]] level of theory. Our calculation at RI-TPSS/def2-SVP level also showed that the transformation is unfavorable by 16.9 kcal mol^{-1}. This is a significant amount of energy, but appropriate ligation or solvation can facilitate this transformation. They have determined

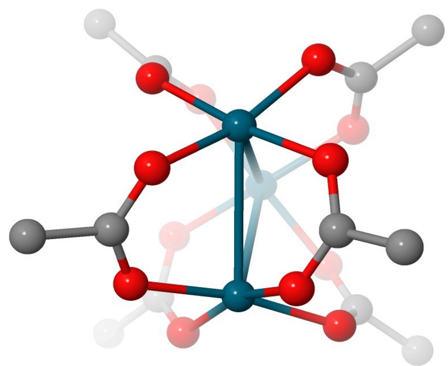

Avg Geometric Parameters

	Gas Phase TPSS/def2-SVP	Exp (CH_2Cl_2)
Pd -- Pd	3.11Å	3.17 Å
Pd -- O	2.02Å	2.00 Å
O-Pd-O	89.2°	89.1°

Figure 1: Comparison of average geometric parameters with crystal structure data for $[Pd(OAc)_2]_3$. Hydrogens are not shown for clarity.

several possible structures of dimeric Pd-acetate and shown that the bridging acetate ligands increase the stability of the dimer. In this study, we have chosen the bridged structure as it is the most thermodynamically stable one and calculated the dimerization energy from the monomeric $Pd(OAc)_2$, as shown in Figure 2.

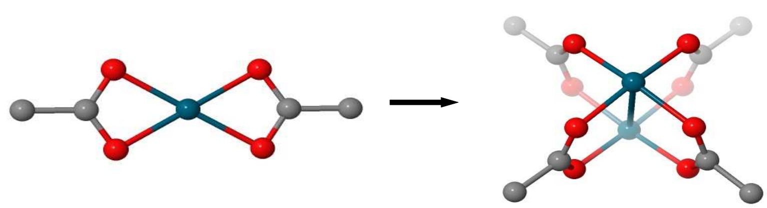

$\Delta G_{dimerization}$	:	--	-32.3 kcal mol^{-1}
$D_{pd—Pd}$(Å)	:	--	2.60
$D_{pd—O}$(Å)	:	2.06	2.02
O--Pd--O	:	63.6°	89.2°

Figure 2: Free energy of dimerization (kcal mol^{-1} and relevant geometric parameters of the monomeric and dimeric Pd acetate.

The DFT calculations on $[Pd(OAc)_2]_2$ show that the highest occupied MO is the antibonding dσ^* formed mainly by the two dz^2 orbitals of the two square planner Pd atoms (Figure 3) while the LUMO is constructed by the mixture of metal d_{xy} orbital and ligand orbitals. Although Pd dz^2 has a significant contribution in the HOMO, small contributions from 5s and 5p_z orbital are also present due to the symmetry-allowed mixing of the 5s and 5p_z orbitals with the metal dz^2 orbital. Similar mixing is found in MO 72, where two Pd dz^2 orbitals have bonding interaction with a minor contribution from 5s and 5p_z orbitals of the metal. As expected, the contributions from 5s and 5p_z orbital are small due to the differences in orbital energies. The orbital mixing leads to the overall increase in the bonding interaction and a decrease in the antibonding interaction. As a result, Pd-Pd has a weak σ bonding interaction. This observation is supported by the Wiberg bond index (WBI[41]) calculation – WBI(Pd-Pd) is 0.17.

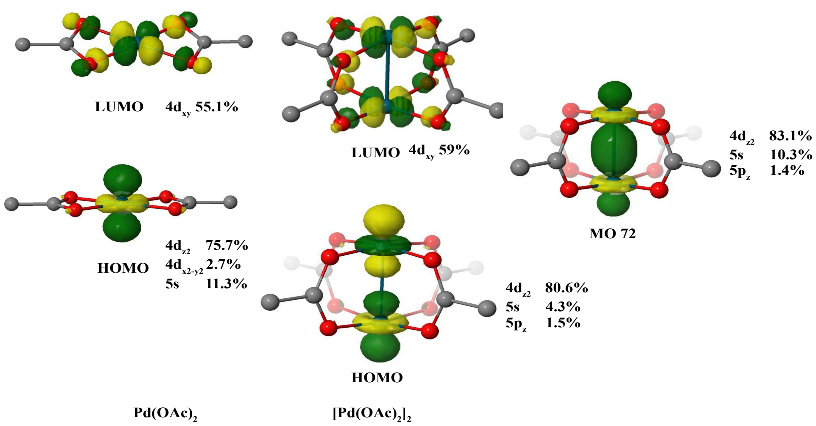

Figure 3: Selected MOs of the Pd(OAc)$_2$ and [Pd(OAc)$_2$]$_2$. Metal orbital compositions are given.

Stepwise degradation of the dimeric [Pd(OAc)$_2$]$_2$ with PH_3 and PPh_3

Steps 1 and 2

We have investigated the step-by-step formation of monomeric Pd species from Pd acetate dimer. Our model system is one Pd-acetate dimer molecule and four ligands (simple phosphine PH_3 or triphenylphosphine PPh_3); ligand molecules get attached with two Pd centers subsequently. In our discussions, the asymptotic limit corresponds to these non-interacting species (Pd acetate dimer and four PH_3/PPh_3). All relative energies are with respect to the sum of the energies of these molecules.

In the starting [Pd(OAc)$_2$]$_2$ complex, the four acetate ligand chelates the two metal centers; hence two Pd centers separately have fulfilled their four coordination. Each metal center exists in an approximate square planner environment. Initially, PH_3 forms a preliminary complex with the dimer (Pd1-P1 distance = 2.9 Å) without any energy barrier, and the stabilization energy(ΔE) is -5.54 kcal mol^{-1}. The further approach of PH_3 passes through the transition state TS-1 with an energy barrier of 7.52 kcal mol^{-1} with respect to A_0. In TS-1, the Pd1-P1 bond distance is 2.68 Å. The attachment of the PH_3 to the Pd1 center is an energetically easy process that results in the complete breaking of the weak Pd1-O1 bond, as observed in the resulting intermediate A_2. The new Pd1-P1 distance is

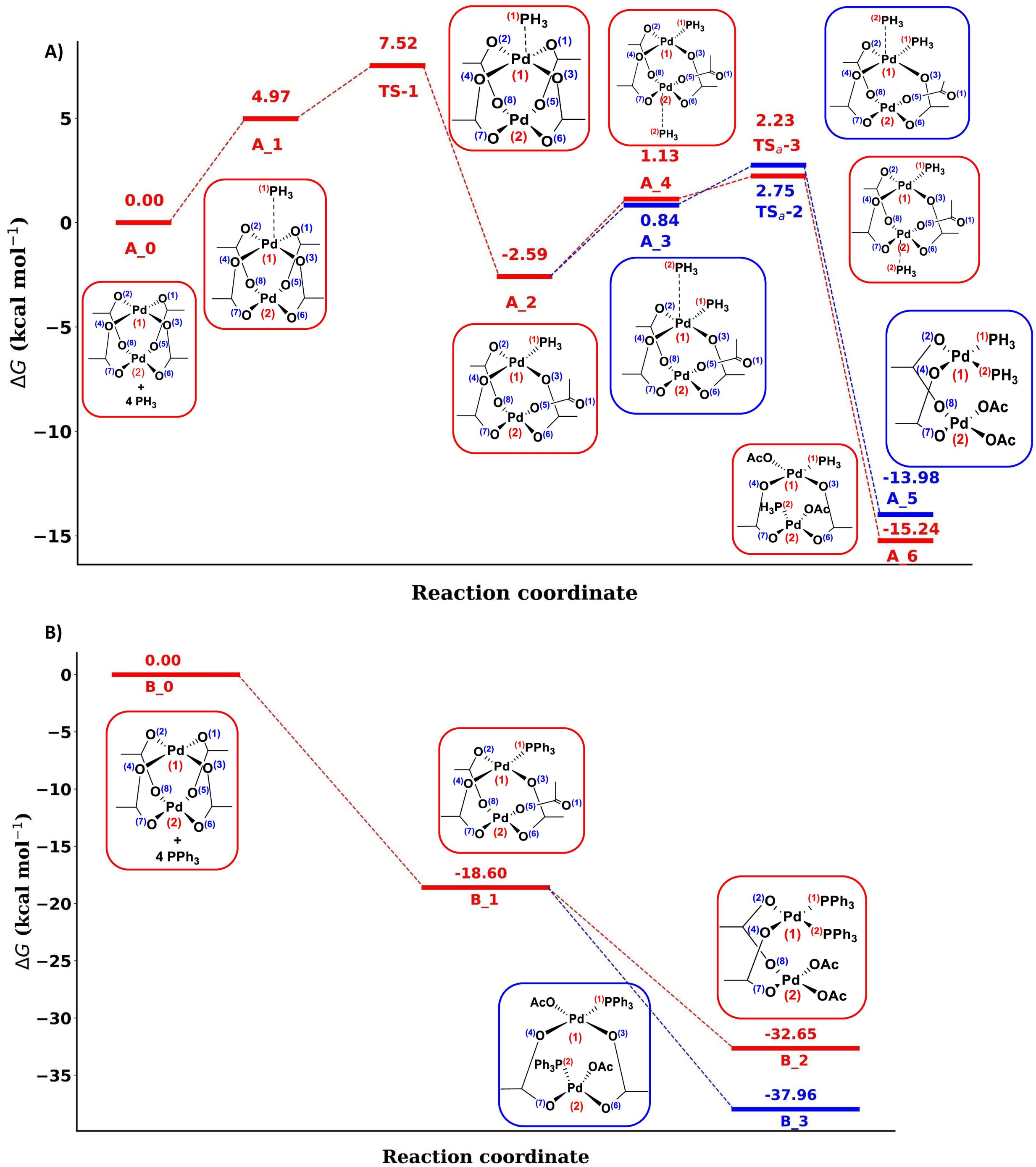

Figure 4: Free energy profile diagram for the first and second addition of A) PH_3 and B) PPh_3 to dimer species calculated at TPSS/def2-SVP level theory.

2.24 Å. The binding of the first PH_3 to the Pd1 center gives stabilization energy of -7.56 kcal mol^{-1} with respect to A_1 and -2.59 kcal mol^{-1} with respect to A_0. On the other hand, the first addition of PPh_3 to the dimer forms the first intermediate B_1 without any barrier. The complexation is highly exergonic (-18.6 kcal mol^{-1}) with respect to B_0. The new Pd1-P1 distance is 2.25 Å in the intermediate B_1.

Adding the second PH_3 to A_2 resulted in two intermediates, A_3 and A_4. In A_3 intermediate, the new incoming PH_3 approaches the Pd to which the first PH_3 is attached (Pd1), whereas, in A_4, the new PH_3 approaches the other Pd center (Pd2). In both cases, the weakly bound preliminary complexes A_3 and A_4 form without any energy barrier. Both these complexes are stabilized (ΔE) compared to A_2 by -5.53 kcal mol^{-1} and -7.05 kcal mol^{-1} for A_3 and A_4, respectively. The bond formation of PH_3 to Pd proceeds through transition states, TS-2 and TS-3. The TS-2 and TS-3 are 2.75 kcal mol^{-1} and 2.23 kcal mol^{-1} higher in energy than A_0, respectively. The TS-2 is slightly higher in energy than the TS-3 (1.90 vs. 1.09 kcal mol^{-1}). This difference may be attributed to the higher steric demand to add a second PH_3 to the same Pd1 center. However, in the case of PPh_3, a situation similar to the first addition of PPh_3 arises. Two intermediates, B_2 and B_3, formed without any energy barrier. In B_2, the second PPh_3 is attached with the same Pd1 center and B_3 to the other Pd2 center. They are energetically stabilized by -13.45 (B_2) and -19.36 (B_3) kcal mol^{-1} with respect to B_1. Both the first and second addition of PH_3 and PPh_3 are shown in Figure 4(a) and (b), respectively.

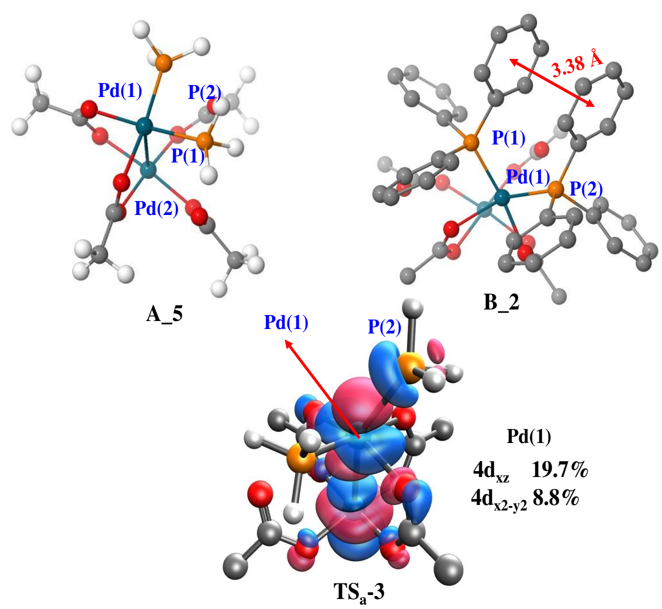

Figure 5: A_5 and B_2 geometry and HOMO of the TS$_a$-3. Hydrogens are not shown for clarity.

In A_5 and B_5 intermediates, where both the PH_3 ligand is attached to the same Pd1 center, their orientation is *cis* to each other (shown in Figure 5). In B_2, the distance between two phenyl rings of the adjacent PPh_3 is 3.38 Å suggesting that the $\pi-\pi$ stacking stabilized the *cis* position of two PPh_3 although PPh_3 is a bulky ligand and there is no transition state barrier. The NCI plot (shown in SI Figure S1) also confirms the $\pi-\pi$ interaction(shown in SI). As we identified the transition state of A_5 formation (TS_a-3), we looked at the HOMO of the transition state. The Pd(1) center is mainly composed of $4d_{xz}$ (19.7%) orbital. The incoming PH_3 (sp^3 bonding orbital) has initially antibonding interaction with the Pd1's $4d_{xz}$ orbital. To make the bonding stable, the PH_3 has to be moved to the side lobe of the $4d_{xz}$ orbital, and that leads to the *trans* orientation relative to the first PH_3. We also expect the same scenario in the case of PPh_3.

Step 3 and 4

In the third step, the new incoming PH_3 forms two preliminary complexes. In A_7, the new PH_3 is attached to the Pd1 center, while in A_9, it is attached to the Pd2 center. The stabilization (ΔE in kcal mol^{-1}) energy for A_7 and A_9 are -7.67 and -6.97. However, the stepwise ΔG is 7.00 kcal mol^{-1} and 3.16 kcal mol^{-1} due to unfavorable entropic factors. The Pd1-P3 distance is 3.14 Å in A_7, and the Pd2-P3 distance is 3.17 Å in A_9. These two preliminary complexes pass through the transition states TS_a-4 and TS_a-5 before forming the intermediates A_10 and A_12, respectively. The barrier heights for TS_a-4 and TS_a-5 are 10.4 kcal mol^{-1} and 9.84 kcal mol^{-1}. In TS_a-4 transition state, the new incoming PH_3 (Pd1-P3 distance 2.54 Å) replaces Pd1-O2 (2.47 Å) linkage whereas in TS_a-5 (Pd2-P3 distance 2.51 Å) PH_3 replaces the Pd2-O7(2.48 Å) bond. The third step, the addition of PH_3 to both the A_5 and A_6 complexes, is endothermic. The reaction energies are 6.01 kcal mol^{-1} and 7.55 kcal mol^{-1}.

In contrast to the first and second insertions of PPh_3, the third PPh_3 forms two preliminary complexes with B_2 (B_7 and B_8). New PPh_3 is attached to the Pd1 center in B_7, whereas in B_8, it is attached to the Pd2 center. The Pd1-P3 distance is 3.87 Å in B_7, and Pd2-P3 distance is 2.68 Å in B_8. As two PPh_3 already attached to the Pd1 center in B_7, the Pd1-P3 distance is higher than the Pd2-P3 distance in B_8. The stabilization energies for these two complexes are almost the same (ΔE -22.02 kcal mol^{-1} and -20.08 kcal mol^{-1}, respectively). However, from another intermediate B_3, only preliminary complex B_6 is formed. Adding new PPh_3 to the Pd2 center in B_3 intermediate will eventually lead to the same preliminary complex because both Pd centers are already attached with one PPh_3 each. The Pd1-P3 distance becomes 3.41 Å in the B_6 intermediate. These prelimi-

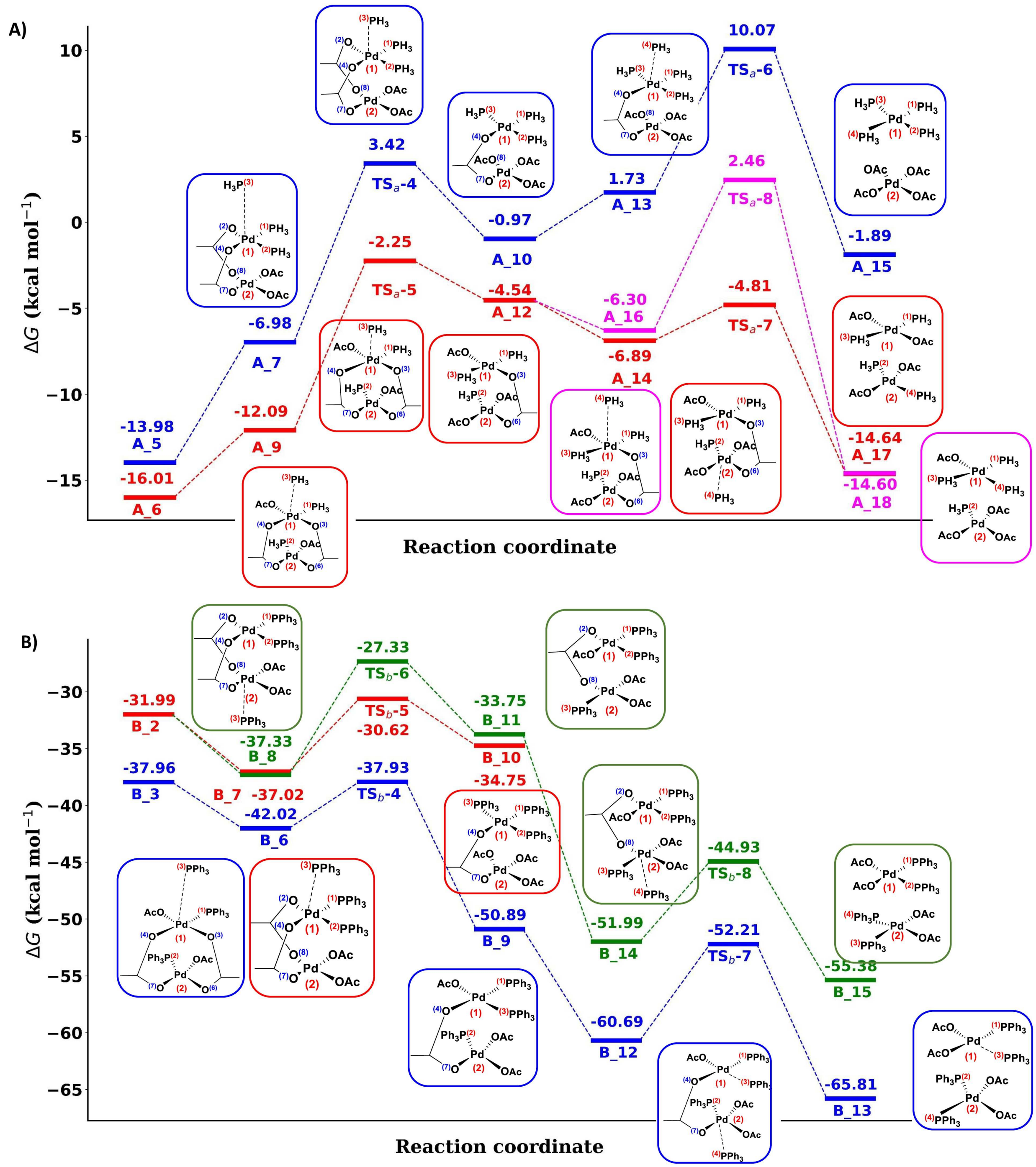

Figure 6: Free energy profile diagram for the third and fourth addition of A) PH_3 and B) PPh_3 to dimer species calculated at TPSS/def2-SVP level theory.

nary complexes form the intermediates B_10, B_11, and B_9 through the transition states TS_b-5, TS_b-6, and TS_b-4, with the barriers 6.40 kcal mol^{-1}, 10.00 kcal mol^{-1}, and 4.09 kcal mol^{-1}, respectively. This step is slightly endergonic for B_7 and B_8 (2.27 kcal mol^{-1} and 3.58 kcal mol^{-1}) but exergonic for B_6 (-8.87 kcal mol^{-1}). In the transition states TS_b-5, TS_b-6 and TS_b-4 the Pd-P3 distances are 2.84 Å, 2.54 Å, and 3.04 Å, respectively.

The Next step is the insertion of the fourth PH_3/PPh_3 with their respective third step intermediates. In the PH_3 case, we have got one preliminary complex A_13 from the A_10 and two preliminary complexes A_15 and A_16, from the A_12. In A_13, the fourth PH_3 will be attached with the Pd1 center, which possesses three PH_3. Similarly, PH_3 can attach with Pd1 and Pd2 center with A_12 intermediate. Attachment with Pd1 gives A_16, and Pd2 gives A_15. In these three preliminary complexes, the Pd-P4 distance has become 3.17 Å, 3.40 Å, and 3.44Å for A_13, A_15, and A_16, respectively. The corresponding transition states are TS_a-6, TS_a-7, and TS_a-8) for forming A_15, A_17, and A_18. Pd1-P4 bond lengths are 2.73 Å and 2.70 Å in TS_a-6 and TS_a-8, and Pd2-P4 bond length is 2.82 Å in TS_a-7. The stepwise barriers for forming A_15, A_17, and A_18 are 8.34 kcal mol^{-1}, 2.08 kcal mol^{-1}, and 8.76 kcal mol^{-1}, respectively. Among these three pathways, TS_a-6 is the energetically highest (from A_13) due to the increase of steric demand at the Pd1 center, where already three PH_3 are present. A similar situation arises in the case of TS_a-8, where two PH_3 are already present at the Pd1 center. TS_a-7 is the lowest among these three. Here the fourth PH_3 attached trans to another PH_3 at the Pd2 center.

In the fourth step of the PPh_3 path, we got two preliminary complexes, B_12 (from B_9) and B_14 (from B_11). We have not proceeded with the B_10 intermediate because three large PPh_3 at the Pd1 center prevent further addition of PPh_3. Both these intermediates are different only in conformations. The fourth PPh_3 will be attached at the Pd2 center because of the less steric congestion in this metal center. The Pd2-P4 distances are 3.31 Å and 3.11 Å for B_12 and B_14. Finally, they pass through transition state TS_b-7 and TS_b-8 before forming the products B_13 and B_15, respectively. At the transition states TS_b-7 and TS_b-8, the Pd2-P4 distances are 2.65 Å and 2.60 Å. The stepwise barriers for the two paths are similar, 8.48 kcal mol^{-1} for TS_b-7 and 7.06 kcal mol^{-1} for TS_b-8. The TS_b-7 is the lower energy path than TS_b-8

After the fourth insertion of PH_3/PPh_3, we got monomeric products. In the PH_3 path, TS_a-6 leads to two monomeric species (A_15) $Pd(PH_3)_4$ and $Pd(OAc)_4$, and TS_a-7 leads to two symmetric monomeric species $Pd(PH_3)_2(OAc)_2$. Similarly, TS_a-8 yields two unsymmetric monomeric products $Pd(PH_3)_3(OAc)$ and $Pd(OAc)_3(PH_3)$. On the other hand, in PPh_3 path, both TS_b-7 and TS_b-8 lead to the formation of the same monomeric species $Pd(PPh_3)_2(OAc)_2$.

Stochastic Kinetic Simulation

As three monomeric species are possible (A_15, A_17, and A_18) in the PH_3 degradation path, we simulated the kinetics with our SSA code to understand the preferences among these paths. The reaction mixture volume is set to unity, and dt is fixed at a low value of 0.0001. In a typical quantum chemical consecutive reaction path, the reactive intermediate species usually undergo some conformational change or form a weak association complex with another reactive species before going to the next transition state. It is often pretty hard to locate the transition state for these small conformational changes or the formation of weak association complexes. These steps might be controlled by the solvent system (via diffusion). In our case, between two transition states, the intermediate forms a week preliminary complex with the incoming PH_3 before going to the next transition state. Here we estimated such energy barriers based on the relative energy of the higher energy intermediate among two consecutive intermediates. We also varied the temperature and the initial population of the starting species to observe the change in the kinetics of the whole process.

Temperature Variation

We have studied the effects of temperature variation in this chemical process. Here, we fixed the initial populations of dimer and PH_3 to 2000 and 4500, respectively, and the number of MC steps to 5000000. We simulated at four different temperatures 298K, 323K, 353K, and 373K. In general, we observed an increase in reaction rate with an increase in temperature from our SSA run (shown in Figure 7). As we increase the temperature from 298K to 373K, the population of A_18 increases rapidly, while the population of A_15 decreases more quickly at the higher temperature. However, at a higher temperature, the population of A_15 remains zero. It suggests that the A_15 might be found in a minute amount in the experimental condition.

Variation of initial population

To understand the effect of the initial population, we varied the dimer: PH_3 ratio from 1:1 to 1:5. We set the temperature to $100°C$ (373K), and the number of MC steps is fixed at 5000000. We have not observed any products population in 1:1 and 1:2 of dimer: PH_3 ratio. Here the populations of various intermediates increase only. The population ratios are shown in Table 1 for 1:3 to 1:5 dimer:PH_3 ratio.

We have seen that increasing the population of PH_3 increases the population of A_15

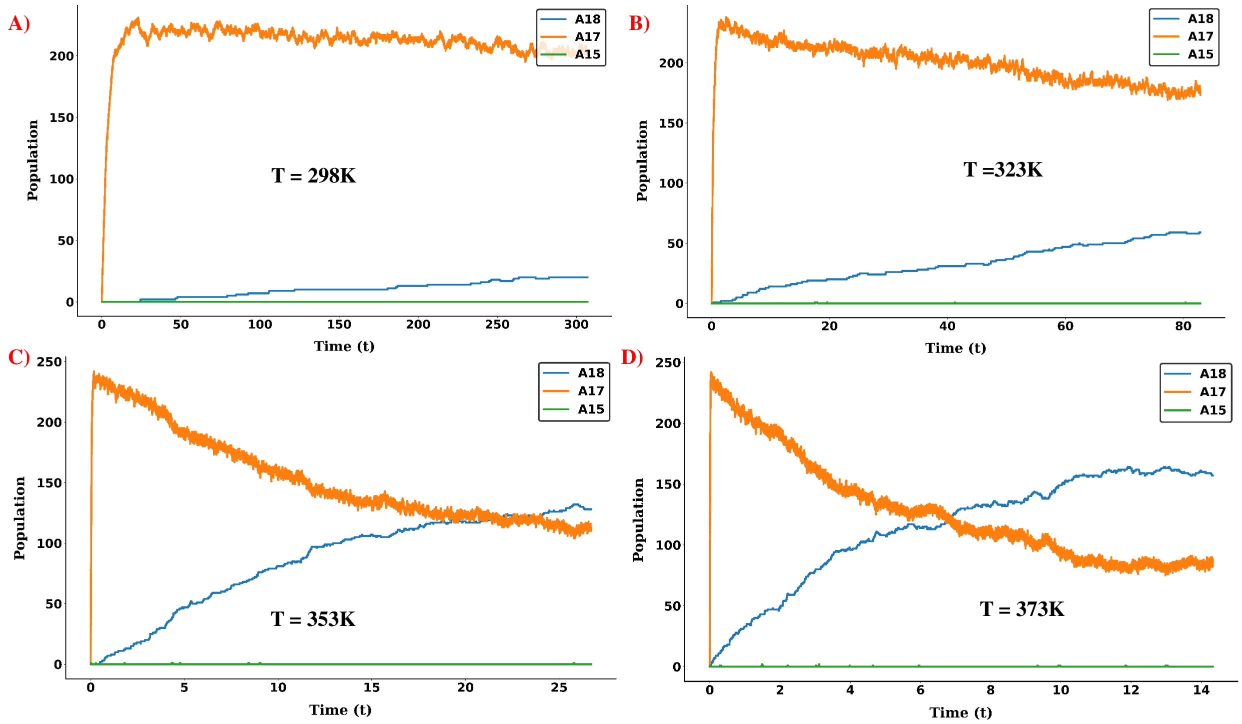

Figure 7: Temperature variation study of the stochastic simulation.

Table 1: Initial population variation of the kinetic simulation

Initial population		**Final population**		
$[Pd(OAc)_2]_2$	**PH_3**	**A_15**	**A_17**	**A_18**
1000	3000	0	243	235
1000	4000	8	490	242
1000	5000	41	463	271

and A_18 while the A_17 population is slowly decreasing with the same number of MC steps. The time evolutions of the products are plotted in Figure 8.

Although with the increases of PH_3 population, some population of PH_3 remains unreactive in the final population of the system, it also increases the population of minor product A_15 . These results suggest that an excess amount of PH_3 is required for the degradation path. As seen in Table 1, the A_15 is a minor product because of the overall higher energy path in the system.

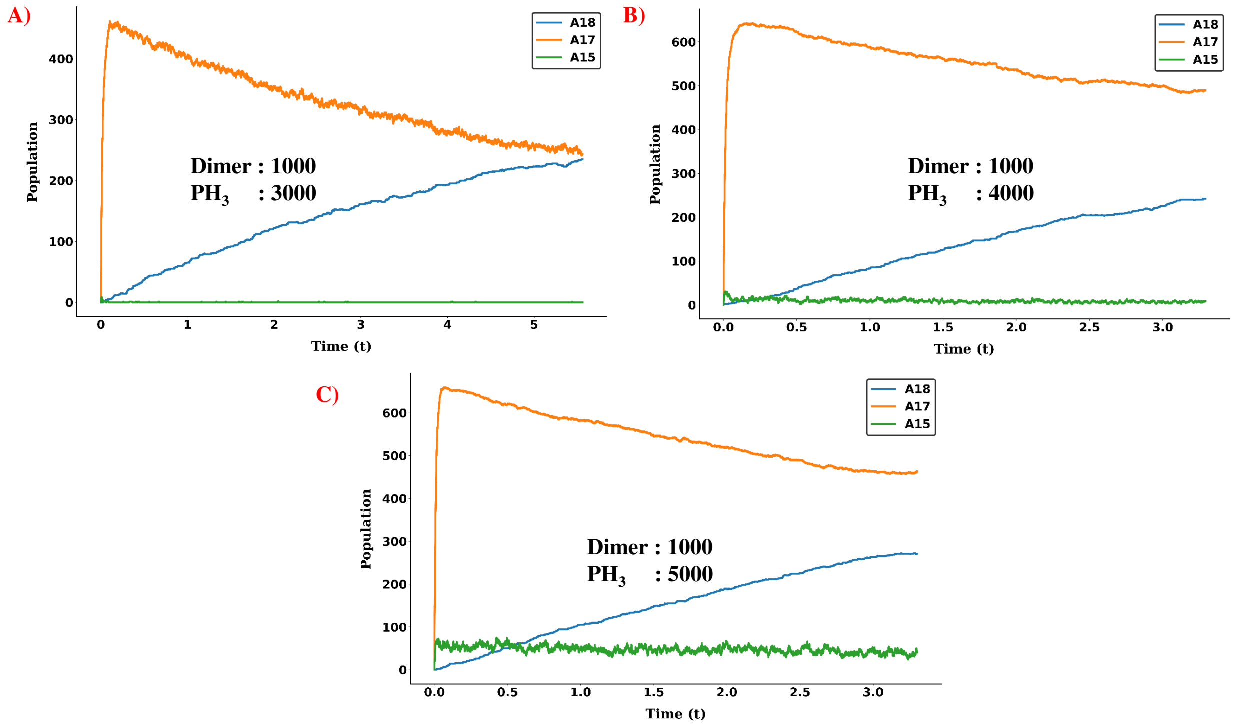

Figure 8: Initial population variation study of the stochastic simulation.

Active Catalytic Species

After the fourth PH_3 addition to the Pd acetate dimer, we got several types of monomeric species. On the other hand, we got one type of monomeric species in the case of PPh_3 addition path. These monomeric species will generate the active catalyst species that can begin the catalytic cycle. From A_15, we got two monomeric species $Pd(OAc)_4$, and $Pd(PH_3)_4$. Now in $Pd(PH_3)_4$ is an active catalyst precursor. Here Pd is in 0 oxidation state, and it is an $18e$ species. To become an active catalyst, it has to be at least $16e$ species. So it can dissociate one PH_3 ligand and behave as an active catalyst. On the other hand, further PH_3 ligand addition is required to replace the acetate from $Pd(OAc)_4$ to form active catalyst. From another intermediate A_17, two same monomeric species is generated, *trans*-$Pd(PH_3)_2(OAc)_2$. Similar type of species was also found by Amatore et al.[11] shown in the Equation 1 in their study of the reaction between monomeric $Pd(OAc)_2$ with PPh_3. Computationally the details formation of active catalyst from this species was also reported from our group.[42] From A_18 intermediate we got $[Pd(PH_3)_3(OAc)]^-$ and $Pd(PH_3)(OAc)_3$. The second species can also be converted to the first one by the addition of excess PH_3 ligand. The first type species $[Pd(PH_3)_3(OAc)]^-$ shown in Figure 9(C) also reported in the formation of active catalyst in Equation 1. In Figure 9, all the potential active catalytic species are shown. Our stochastic simulation reveals that A_15 and A_18 intermediates can form in a major amount.

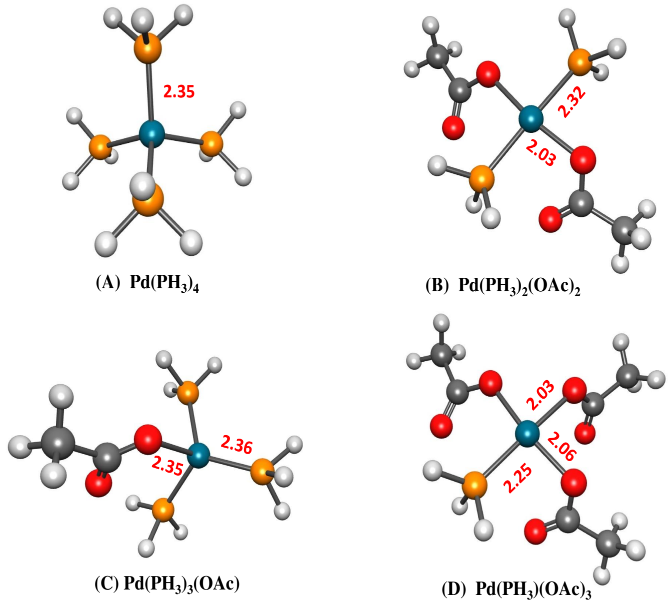

Figure 9: Monomeric species after the fourth addition of PH_3 to the dimer. All the bond lengths are in Å unit.

On the other side, from the PPh_3 path, after the fourth addition, two same monomeric species $Pd(PPh_3)_2(OAc)_2$ is formed (Shown in Figure 10). Here two PPh_3 ligands are *cis* to each other. However, Amatore et al.,[11] from their experiment, reported the *trans* form of this species when they started from monomeric Pd-acetate. This *cis* species can be converted to $Pd(PPh_3)_3(OAc)^-$ by exchanging one acetate ligand with PPh_3 and forming the active catalytic species, although we have not explored this path.

Conclusions

Several experimental studies indicate that depending on reaction conditions, the $[Pd(OAc)_2]_2$ might be a resting state of the Pd-acetate in the coupling reaction. We have studied the degradation path of the dimer with the addition of both PH_3 and PPh_3 ligands with the help of our automated reaction search method. Our study indicates that the degradation of $[Pd(OAc)_2]_2$ can also generate similar types of active catalytic species, which were reported earlier starting from the Pd-acetate monomer. Smaller ligands, e.g., PMe_3 should follow the PH_3 degradation path while bulky ligands, e.g., PCy_3 can take the PPh_3 degradation route. In addition, we also explored the bonding characteristics of $[Pd(OAc)_2]_2$. We introduced a new implementation of Gillespie stochastic simulation and applied it to

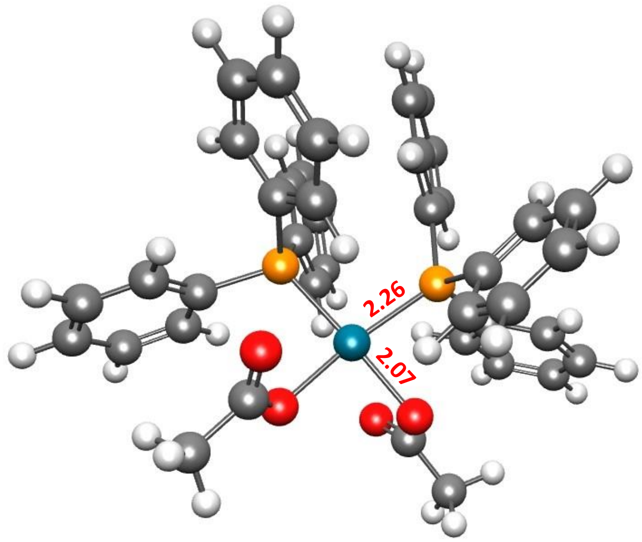

***cis*-Pd(PPh$_3$)$_2$(OAc)$_2$**

Figure 10: Monomeric species after the fourth addition of PPh_3 to the dimer. All the bond lengths are in Å unit.

the degradation path. We believe our SSA code can give more insights into the catalytic path where multiple competitive reaction channels are possible. The code is available at `https://github.com/anooplab/ssa`.

Acknowledgement

We acknowledge the National Supercomputing Mission (NSM) for providing computing resources of 'PARAM Shakti' at IIT Kharagpur, which is implemented by C-DAC and supported by the Ministry of Electronics and Information Technology (MeitY) and Department of Science and Technology (DST), Government of India. We thank the SERB grant (EMR/2017/003048) for research funding. We also thank Mr. Debankur Bhattacharyya, who has started developing the code during his master project.

Notes

The authors declare no competing financial interest.

References

(1) Bonney, K. J.; Schoenebeck, F. Experiment and computation: a combined approach to study the reactivity of palladium complexes in oxidation states 0 toiv. *Chem. Soc. Rev.* **2014**, *43*, 6609.

(2) Mirica, L. M.; Khusnutdinova, J. R. Structure and electronic properties of Pd(III) complexes. *Coordination Chemistry Reviews* **2013**, *257*, 299–314.

(3) Rauf, W.; Brown, J. M. Reactive intermediates in catalytic alkenylation; pathways for Mizoroki–Heck, oxidative Heck and Fujiwara–Moritani reactions. *Chem. Commun.* **2013**, *49*, 8430–8440.

(4) Carole, W. A.; Colacot, T. J. Understanding Palladium Acetate from a User Perspective. *Chem. Eur. J.* **2016**, *22*, 7686–7695.

(5) Bakhmutov, V. I.; Berry, J. F.; Cotton, F. A.; Ibragimov, S.; Murillo, C. A. Non-trivial behavior of palladium(ii) acetate. *Dalton Trans.* **2005**, 1989.

(6) Powers, D. C.; Ritter, T. Bimetallic Pd(III) complexes in palladium-catalysed carbon–heteroatom bond formation. *Nature Chem* **2009**, *1*, 302–309.

(7) Mazzotti, A. R.; Campbell, M. G.; Tang, P.; Murphy, J. M.; Ritter, T. Palladium(III)-Catalyzed Fluorination of Arylboronic Acid Derivatives. *J. Am. Chem. Soc.* **2013**, *135*, 14012–14015.

(8) Canty, A. J.; Ariafard, A.; Sanford, M. S.; Yates, B. F. Mechanism of Pd-Catalyzed Ar–Ar Bond Formation Involving Ligand-Directed C–H Arylation and Diaryliodonium Oxidants: Computational Studies of Orthopalladation at Binuclear Pd(II) Centers, Oxidation To Form Binuclear Palladium(III) Species, and Ar···Ar Reductive Coupling. *Organometallics* **2013**, *32*, 544–555.

(9) Proutiere, F.; Aufiero, M.; Schoenebeck, F. Reactivity and Stability of Dinuclear Pd(I) Complexes: Studies on the Active Catalytic Species, Insights into Precatalyst Activation and Deactivation, and Application in Highly Selective Cross-Coupling Reactions. *J. Am. Chem. Soc.* **2011**, *134*, 606–612.

(10) Cook, A. K.; Sanford, M. S. Mechanism of the Palladium-Catalyzed Arene C–H Acetoxylation: A Comparison of Catalysts and Ligand Effects. *J. Am. Chem. Soc.* **2015**, *137*, 3109–3118.

(11) Amatore, C.; Jutand, A. Anionic Pd(0) and Pd(II) Intermediates in Palladium-Catalyzed Heck and Cross-Coupling Reactions. *Acc. Chem. Res.* **2000**, *33*, 314–321.

(12) Kozuch, S.; Shaik, S.; Jutand, A.; Amatore, C. Active Anionic Zero-Valent Palladium Catalysts: Characterization by Density Functional Calculations. *Chem. Eur. J.* **2004**, *10*, 3072–3080.

(13) Bottoni, A.; Carvajal, M. A.; Miscione, G. P.; Novoa, J. J. A theoretical investigation of the oxidation states of palladium complexes and their role in the carbonylation reaction. *Molecular Physics* **2010**, *108*, 1619–1640.

(14) Zhang, L.-L.; Zhang, L.; Li, S.-J.; Fang, D.-C. DFT studies on the distinct mechanisms of C–H activation and oxidation reactions mediated by mononuclear- and binuclear-palladium. *Dalton Trans.* **2018**, *47*, 6102–6111.

(15) Bay, K. L.; Yang, Y.-F.; Houk, K. Multiple roles of silver salts in palladium-catalyzed C–H activations. *Journal of Organometallic Chemistry* **2018**, *864*, 19–25.

(16) Nandi, S.; McAnanama-Brereton, S. R.; Waller, M. P.; Anoop, A. A tabu-search based strategy for modeling molecular aggregates and binary reactions. **2017**, *1111*, 69–81.

(17) Maeda, S.; Ohno, K.; Morokuma, K. An Automated and Systematic Transition Structure Explorer in Large Flexible Molecular Systems Based on Combined Global Reaction Route Mapping and Microiteration Methods. *J. Chem. Theory Comput.* **2009**, *5*, 2734–2743.

(18) Maeda, S.; Morokuma, K. Communications: A systematic method for locating transition structures of A+B→X type reactions. *The Journal of Chemical Physics* **2010**, *132*, 241102.

(19) Gillespie, D. T. Stochastic Simulation of Chemical Kinetics. *Annu. Rev. Phys. Chem.* **2007**, *58*, 35–55.

(20) Bannwarth, C.; Caldeweyher, E.; Ehlert, S.; Hansen, A.; Pracht, P.; Seibert, J.; Spicher, S.; Grimme, S. Extended tight-binding quantum chemistry methods. **2020**, *11*.

(21) Grimme, S.; Bannwarth, C.; Shushkov, P. A Robust and Accurate Tight-Binding Quantum Chemical Method for Structures, Vibrational Frequencies, and Noncovalent Interactions of Large Molecular Systems Parametrized for All spd-Block Elements (Z = 1–86). *J. Chem. Theory Comput.* **2017**, *13*, 1989–2009.

(22) Furche, F.; Ahlrichs, R.; Hättig, C.; Klopper, W.; Sierka, M.; Weigend, F. Turbomole. **2013**, *4*, 91–100.

(23) Becke, A. D. Density-functional exchange-energy approximation with correct asymptotic behavior. *Phys. Rev. A* **1988**, *38*, 3098–3100.

(24) Grimme, S.; Antony, J.; Ehrlich, S.; Krieg, H. A consistent and accurate ab initio parametrization of density functional dispersion correction (DFT-D) for the 94 elements H-Pu. *The Journal of Chemical Physics* **2010**, *132*, 154104.

(25) Henkelman, G.; Uberuaga, B. P.; Jónsson, H. A climbing image nudged elastic band method for finding saddle points and minimum energy paths. **2000**, *113*, 9901–9904.

(26) Neese, F. Software update: the ORCA program system, version 4.0. **2017**, *8*.

(27) Eichkorn, K.; Weigend, F.; Treutler, O.; Ahlrichs, R. Auxiliary basis sets for main row atoms and transition metals and their use to approximate Coulomb potentials. *Theoretical Chemistry Accounts: Theory, Computation, and Modeling (Theoretica Chimica Acta)* **1997**, *97*, 119–124.

(28) Tao, J.; Perdew, J. P.; Staroverov, V. N.; Scuseria, G. E. Climbing the Density Functional Ladder: Nonempirical Meta–Generalized Gradient Approximation Designed for Molecules and Solids. *Phys. Rev. Lett.* **2003**, *91*.

(29) Weigend, F.; Ahlrichs, R. Balanced basis sets of split valence, triple zeta valence and quadruple zeta valence quality for H to Rn: Design and assessment of accuracy. *Phys. Chem. Chem. Phys.* **2005**, *7*, 3297.

(30) Grimme, S.; Ehrlich, S.; Goerigk, L. Effect of the damping function in dispersion corrected density functional theory. *J. Comput. Chem.* **2011**, *32*, 1456–1465.

(31) Xu, X.; Truhlar, D. G. Accuracy of Effective Core Potentials and Basis Sets for Density Functional Calculations, Including Relativistic Effects, As Illustrated by Calculations on Arsenic Compounds. *J. Chem. Theory Comput.* **2011**, *7*, 2766–2779.

(32) Reed, A. E.; Weinstock, R. B.; Weinhold, F. Natural population analysis. *The Journal of Chemical Physics* **1985**, *83*, 735–746.

(33) Lu, T.; Chen, F. Multiwfn: A multifunctional wavefunction analyzer. *J. Comput. Chem.* **2011**, *33*, 580–592.

(34) Frisch, M. J. et al. Gaussian~16 Revision C.01. 2016; Gaussian Inc. Wallingford CT.

(35) Haines, B. E.; Berry, J. F.; Yu, J.-Q.; Musaev, D. G. Factors Controlling Stability and Reactivity of Dimeric Pd(II) Complexes in C–H Functionalization Catalysis. *ACS Catal.* **2016**, *6*, 829–839.

(36) Zhao, Y.; Truhlar, D. G. The M06 suite of density functionals for main group thermochemistry, thermochemical kinetics, noncovalent interactions, excited states, and transition elements: two new functionals and systematic testing of four M06-class functionals and 12 other functionals. *Theor Chem Account* **2007**, *120*, 215–241.

(37) Petersson, G. A.; Bennett, A.; Tensfeldt, T. G.; Al-Laham, M. A.; Shirley, W. A.; Mantzaris, J. A complete basis set model chemistry. I. The total energies of closed-shell atoms and hydrides of the first-row elements. *The Journal of Chemical Physics* **1988**, *89*, 2193–2218.

(38) Hay, P. J.; Wadt, W. R. Ab initio effective core potentials for molecular calculations. Potentials for the transition metal atoms Sc to Hg. *The Journal of Chemical Physics* **1985**, *82*, 270–283.

(39) Wadt, W. R.; Hay, P. J. Ab initio effective core potentials for molecular calculations. Potentials for main group elements Na to Bi. *The Journal of Chemical Physics* **1985**, *82*, 284–298.

(40) Hay, P. J.; Wadt, W. R. Ab initio effective core potentials for molecular calculations. Potentials for K to Au including the outermost core orbitals. *The Journal of Chemical Physics* **1985**, *82*, 299–310.

(41) Wiberg, K. Application of the pople-santry-segal CNDO method to the cyclopropylcarbinyl and cyclobutyl cation and to bicyclobutane. *Tetrahedron* **1968**, *24*, 1083–1096.

(42) Rao, D. Y.; Anoop, A. Density Functional Theory study on the formation of the active catalysts in palladium catalysed reaction. *The Journal of Indian Chemical Society* **2019**, *96*, 909–919.